Physics Letters A 474 (2023) 128830

Contents lists available at ScienceDirect

Physics Letters A

journal homepage: www.elsevier.com/locate/pla

Tuning the van Hove singularities in monolayer PbBiI via C_{3v} symmetry breaking

Tran C. Phong [a,b,*], Nguyen T. Nam [c], Le T.T. Phuong [d]

[a] Atomic Molecular and Optical Physics Research Group, Advanced Institute of Materials Science, Ton Duc Thang University, Ho Chi Minh City, Viet Nam
[b] Faculty of Electrical and Electronics Engineering, Ton Duc Thang University, Ho Chi Minh City, Viet Nam
[c] Department of Physics, Faculty of Mechanical Engineering, Hanoi University of Civil Engineering, Hanoi, Viet Nam
[d] Faculty of Physics, University of Education, Hue University, Hue City, Viet Nam

ARTICLE INFO

Article history:
Received 24 February 2023
Received in revised form 4 April 2023
Accepted 4 April 2023
Available online 13 April 2023
Communicated by L. Ghivelder

Keywords:
The van Hove singularity
Fermi energy
Electronic density of states
Green's function

ABSTRACT

Various filling fractions of the van Hove singularities (vHs) in the vicinity of the Fermi energy give rise to exotic phenomena. Here, we tune vHs in a new family member of quantum spin Hall insulators PbBiI via two mechanisms of C_{3v} symmetry breaking; applying an in-plane magnetization exchange field and an inversion symmetry breaking field. Depending on the mechanism and dispersion direction of host electrons, we find Weyl nodes in the electronic band structure, and in turn, bare vHs deform away from the Fermi energy. Moreover, the number of vHs increases due to the reconstruction of the Fermi surface induced by the above mechanisms. Overall, we indeed propose two efficient mechanisms to tune/create vHs for various emergent applications in optoelectronics.

1. Introduction

Quantum spin Hall insulators (QSHIs) with fully spin-polarized helical edge modes lead to important applications for spintronics and low-power information processing based on topological effects [1–4]. Mainly, inherent spin-orbit coupling (SOC) and band inversion in these systems make them interesting in condensed matter physics [5–8]. Upon breaking the inversion symmetry between spin-dependent states, an extrinsic Rashba SOC emerges for chiral spin textures [2,9–11]. Heavy elements such as Bi, Pb, and W are proper candidates for providing novel features because of their strong SOCs [12–16].

Recently, honeycomb lattices of IV, V, and VII elements, e.g., monolayer PbBiI, have proposed novel insights due to the presence of a Rashba-like SOC and an unconventional spin texture [17–22]. The evolution of the Wannier center of charges confirms that PbBiI is a QSHI [17]. In such structures, the time-reversal symmetry protects both the edge and bulk states, which results in less energy loss in practical applications. Similar to conventional QSHIs, the properties of such materials can be controlled by electron-electron interaction [23–29], bias voltage [5,30,31], an external magnetic field [32–36], etc.

In monolayer buckled PbBiI, Pb-Bi bonds weakly stack with I atoms [17,37–39] and the *ab initio* calculations [17,40–42] have presented that the highest valence (lowest conduction) band is mainly originated from the $p_{x,y}$ (p_z)-Bi orbitals, implying that the contribution of Pb-I dimers is negligible. The SOC basis $|J, j_z\rangle$ (with total angular momentum J and spin direction j_z) of Bi atoms mainly determine the effective electronic band structure of PbBiI single-layer. The buckled structure follows from the C_{3v} symmetry including three operators, namely time-reversal symmetry $\mathcal{T} : |J, j_z\rangle \mapsto 2j_z\langle J, j_z|$, threefold rotation symmetry $\mathcal{R}_3 : |J, j_z\rangle \mapsto e^{2\mathrm{i}j_z\pi/3}|J, j_z\rangle$ along the z-axis, and the mirror symmetry $\mathcal{M}_x : |J, j_z\rangle \mapsto -\mathrm{i}|J, j_z\rangle$ in the y-z plane.

According to a recent proposition for C_{3v} symmetry breaking (CSB) protocol on the band engineering of monolayer PbBiI [19], which leads to interesting optical properties, we aim at engineering the van Hove singularities (vHs) around the Fermi energy through two CSB mechanisms. We first apply an in-plane magnetization and then an inversion symmetry-breaking field to see how these fields can be used to tune the location of vHs as well as to induce new vHs. Upon applying CSB fields, the Fermi surface undergoes a large reconstruction and as a result of this, vHs get away from the Fermi energy and it is important to see how they become flat. Here, we mainly focus on the broadening of bands in the presence of CSB fields, which affects all intrin-

* Corresponding author.
E-mail addresses: trancongphong@tdtu.edu.vn (T.C. Phong), lttphuong@hueuni.edu.vn (L.T.T. Phuong).

https://doi.org/10.1016/j.physleta.2023.128830
0375-9601/

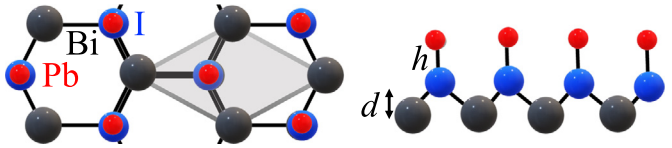

Fig. 1. Top and side views of monolayer PbBiI with the buckled parameter $d \simeq 1.3$ Å and bond length $h = 1.35$ Å. Gray rhombic denotes the unit cell.

sic electronic features of the system. Physically, the emergence of vHs can be understood from the overlap of orbitals between the atoms in a lattice. Depending on the strength of this overlap/hybridization, the broadening of bands will be changed. A flat band is formed from states that have very little orbital overlap between the lattice sites, while parabolic bands mainly stem from strong overlaps. Investigation of vHs is important for optoelectronic applications because the optical absorption spectrum of solid stems from the electronic band structure. Hence, tuning the vHs modifies the optical features.

This paper is organized as follows. In Sec. 2, we present the Hamiltonian model of monolayer PbBiI in the absence and presence of CSB fields. In Sec. 3, we present the numerical results for the electronic band structure and density of states to characterize the Fermi surface and vHs, respectively. Finally, we provide a summary of the paper in Sec. 4.

2. Theory and method

Let us start with the geometry-lattice of monolayer PbBiI in Fig. 1. The buckling parameter and bond length of this structure is $d \simeq 1.3$ Å and $h = 1.35$ Å, respectively. For $S = 1/2$ and the p-orbital angular momentum of $L = 1$ of Bi atoms, the total angular momentum for both spin directions $j_z = \{+1/2, -1/2\}$ is given by $J = \{1/2, 3/2\}$. As mentioned in the introduction, the SOC basis of Bi atoms $|J, j_z\rangle$ mainly forms the Hamiltonian model of the host system. Close to the Γ-point in the first Brillouin zone characterized by the momenta $k_\pm = k_x \pm \mathrm{i}k_y$ and $k = \sqrt{k_x^2 + k_y^2}$, the tight-binding approximation [17] leads to

$$\mathcal{H}_{\vec{k}} = \mathcal{H}_0 + \mathcal{H}_{\rm int}\,, \tag{1}$$

where

$$\mathcal{H}_0 = \begin{pmatrix} -\varepsilon_{12} & 0 & 0 & 0 \\ 0 & -\varepsilon_{12} & 0 & 0 \\ 0 & 0 & +\varepsilon_{32} & 0 \\ 0 & 0 & 0 & +\varepsilon_{32} \end{pmatrix}, \tag{2a}$$

$$\mathcal{H}_{\rm int} = \begin{pmatrix} \zeta_{12}k^2 & \mathrm{i}\alpha_{R,12}k_- & 0 & \gamma k_- \\ -\mathrm{i}\alpha_{R,12}k_+ & \zeta_{12}k^2 & \gamma k_+ & 0 \\ 0 & \gamma k_- & -\zeta_{32}k^2 & 0 \\ \gamma k_+ & 0 & 0 & -\zeta_{32}k^2 \end{pmatrix}, \tag{2b}$$

and $\varepsilon_{12} = 0.1685$ eV, $\varepsilon_{32} = 0.1575$ eV, $\zeta_{12} = 0.008187$ eV/Å^2, $\zeta_{32} = 0.038068$ eV/Å^2, $\alpha_{R,12} = 3.0919$ eV/Å, and $\gamma = -3.5853$ eV/Å are the model parameters from the *ab initio* calculations [17]. In the pristine lattice, we deal with an isotropic electronic band structure including a bulk gap $\mathcal{E}_{\rm g} \simeq 0.275$ eV and a Rashba-like (RL) spin splitting gap $\mathcal{E}_{\rm R} \simeq 0.051$ eV [17–22].

Turning to the CSB fields, we first change the orbital hybridization of Bi orbitals with opposite spin directions $j_z = \{+1/2, -1/2\}$ via an in-plane magnetization field $\mathcal{H}_{\rm M} = \mathcal{F}_{\rm M}\tau_0 \otimes \sigma_x$ (τ_0 stands for the identity matrix in the momentum space and σ_x is the Pauli-x-matrix of spin space), which can be induced to the system by a magnetic dopant or an external magnetic field [43]. Secondly, we turn on two different gauge shifts [44] for inversion symmetry

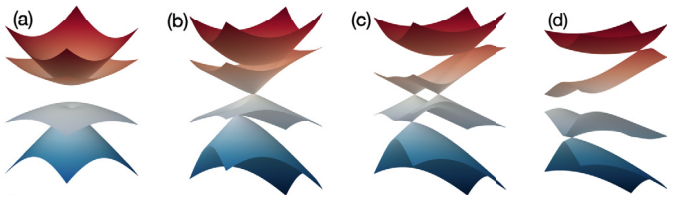

Fig. 2. Dressed band structure of monolayer PbBiI by the in-plane magnetization field at (a) $\mathcal{F}_{\rm M} = 0$ eV, (b) $\mathcal{F}_{\rm M} = 0.5[\varepsilon_{32} + \varepsilon_{12}]$, (c) $\mathcal{F}_{\rm M} = \varepsilon_{32} + \varepsilon_{12}$, and (d) $\mathcal{F}_{\rm M} = 2[\varepsilon_{32} + \varepsilon_{12}]$. Gapless phase and Weyl nodes in (b) and (c), respectively, propose possible electronic phase transitions in PbBiI.

breaking (ISB) between the total angular momenta $J = \{1/2, 3/2\}$ by a field $\mathcal{H}_{\rm ISB} = \mathcal{F}_{\rm ISB}\tau_x \otimes \sigma_x$ (τ_x stands for the Pauli-x-matrix in the momentum space). Hence,

$$\mathcal{H}^{\rm M}_{\vec{k}} = \mathcal{H}_{\vec{k}} + \mathcal{F}_{\rm M}\tau_0 \otimes \sigma_x\,, \tag{3a}$$

$$\mathcal{H}^{\rm ISB}_{\vec{k}} = \mathcal{H}_{\vec{k}} + \mathcal{F}_{\rm ISB}\tau_x \otimes \sigma_x\,, \tag{3b}$$

$$\mathcal{H}^{\mathcal{F}}_{\vec{k}} = \mathcal{H}_{\vec{k}} + \mathcal{F}J_2 \otimes \sigma_x\,, \tag{3c}$$

where in the last term we consider both fields together including $J_2 = \tau_0 + \tau_x$. In the presence of CSB fields, we deal with an anisotropic electronic band structure and dressed bulk and RL gaps. The band structures are obtained by diagonalizing the Hamiltonians [45–48].

To determine the location and intensity of vHs in the absence and presence of CSB fields, we stick to the electronic density of states (DOS) through [49]

$$\mathrm{DOS} = -\frac{1}{\pi}\mathrm{Tr}\sum_{\vec{k}}\mathrm{Im}\big[\mathcal{G}(\vec{k}, \mathcal{E})\big]\,, \tag{4}$$

where $\mathcal{G}(\vec{k}, \mathcal{E}) = [\mathcal{E} + \mathrm{i}\eta - \mathcal{H}^{\rm M/ISB/\mathcal{F}}_{\vec{k}}]^{-1}$ is the Green's function with a phenomenological factor $\eta = 2$ meV. In the electronic DOS, weaker logarithmic divergence (due to the presence of critical $\vec{k}$ points, where $\partial\mathcal{E}/\partial\vec{k} = 0$) corresponds to the vHs [50–52] and we tune the order parameters (bulk gap $\mathcal{E}_{\rm g}$ and RL gap $\mathcal{E}_{\rm R}$) via CSB fields in the Hamiltonians to affect the vHs. We briefly comment that in the presence of disorder fields, the vHs become different. To this end, one needs to use the Dyson equation for the interacting Green's functions employing the T-matrix theory and Born approximation [53].

3. Numerical results

At the Fermi energy and $\vec{k} = 0$, i.e. at the band center of the structure, one only deals with $\mathcal{H}_0$ in Eq. (1) so that we have two degenerate dispersions in both valence and conduction bands. The energy difference between the lowest conduction band $-\varepsilon_{12}$ and highest valence band ε_{32} is simply given by $\varepsilon_{32} + \varepsilon_{12} \simeq 0.326$ eV. As a benchmark, we would vary the fields of CSB below, at, and above this energy to see how variability in the position of the vHs with respect to the Fermi level occurs. In what follows, we first look at the electronic band structure for the three regimes abovementioned to see how the Fermi surface (as the main origin of vHs) undergoes the alteration with CSB fields. Second, we continue with the electronic DOS to address vHs.

3.1. $\mathcal{F}_{\rm M}$ effects

In Fig. 2(a), we plot the band structure for pristine monolayer PbBiI. From the bottom to the top, we have first, second, third, and fourth bands. The bulk gap $\mathcal{E}_{\rm g} \simeq 0.275$ eV appears between the second and third ones, while the RL gap $\mathcal{E}_{\rm R} \simeq 0.051$ eV appears between the first and second ones. As soon as we turn on

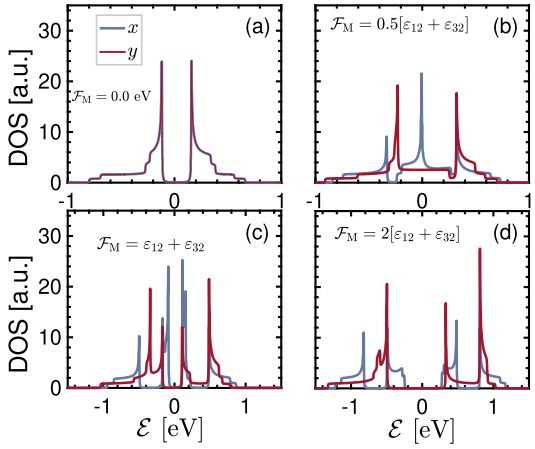

Fig. 3. Dressed electronic DOS of monolayer PbBiI by the in-plane magnetization field at (a) $\mathcal{F}_M = 0$ eV, (b) $\mathcal{F}_M = 0.5[\varepsilon_{32} + \varepsilon_{12}]$, (c) $\mathcal{F}_M = \varepsilon_{32} + \varepsilon_{12}$, and (d) $\mathcal{F}_M = 2[\varepsilon_{32} + \varepsilon_{12}]$. Depending on the dispersion direction of host electrons and the regime of the field with respect to the benchmark energy difference $\varepsilon_{32} + \varepsilon_{12}$, more number of vHs (corresponding to various weak and strong orbital hybridizations between lattice sites) compared to two bare ones in the pristine PbBiI is evident.

the in-plane magnetization field $\mathcal{F}_M = 0.5[\varepsilon_{32} + \varepsilon_{12}]$ in Fig. 2(b), the band structure starts to alter such that both gaps change. Interestingly, the bulk gap vanishes, while the RL gap locates at different momenta than the pristine ones. For $\mathcal{F}_M = \varepsilon_{32} + \varepsilon_{12}$ in Fig. 2(c), two gapless states emerge in the vicinity of the Fermi surface, sol-called Weyl nodes [54–56]. For the third regime, i.e., $\mathcal{F}_M = 2[\varepsilon_{32} + \varepsilon_{12}]$ in Fig. 2(d), the bulk gap reopens at different momenta. In all three regimes, the RL gap still appears at different momenta. Moreover, for all three regimes, the third and fourth bands at higher energies far from the Fermi energy cross each other at a momentum far away from the band center. Although it is easy to plot the Fermi surface of each new band via a contour plot of a certain energy level, a side view of the band structure is adequate to confirm that the Fermi surface is reconstructed by $\mathcal{F}_M$. Such phase transitions due to the gap changes should also manifest themselves in the electronic DOS.

In the pristine monolayer PbBiI, importantly, there are two vHs around the zero Fermi energy isotropically along both x and y directions, as shown in Fig. 3(a). The location of these two singularities varies as the $\mathcal{F}_M$ is applied and accordingly, new vHs emerge. We find that the flatter vHs at $\mathcal{F}_M = 0.5[\varepsilon_{32} + \varepsilon_{12}]$ in Fig. 3(b) is located at the zero energy along the x-direction due to two gapless phases of the system in this regime. Additionally, two more vHs appear in the valence (due to the new RL gap position) and conduction (due to the band-crossing of third and fourth energy bands) sides. While only two vHs take place along the y-direction. In turn, this is a direct consequence of the anisotropic effect of CSB fields on the vHs in monolayer PbBiI. For $\mathcal{F}_M = \varepsilon_{32} + \varepsilon_{12}$ in Fig. 3(c), one immediate result is the appearance of a wider dispersion. Furthermore, six and four vHs are formed along the x- and y-direction, respectively. The higher number of vHs is due to Weyl nodes in this regime such that the flatter vHs again belongs to the x-direction. As mentioned before, the system is re-gapped for $\mathcal{F}_M = 2[\varepsilon_{32} + \varepsilon_{12}]$, so, in Fig. 3(d), the gap around the zero energy is wider and the number of vHs along both directions is doubled. The vHs-doubling effect stems from the curvature of valence and conduction bands which is not the same as the pristine gapped phase. In contrast to two other regimes, this one leads to the flatter vHs along the y-direction. As a general remark, it is necessary to point out that the bulk gap along both directions increases with $\mathcal{F}_M \geq \varepsilon_{32} + \varepsilon_{12}$. In terms of orbital hybridization in the presence of $\mathcal{F}_M$, it is also worth mentioning that the orbitals of lattice sites

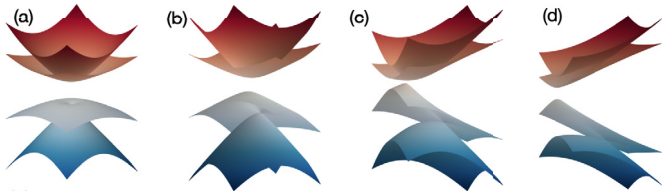

Fig. 4. Dressed band structure of monolayer PbBiI by the ISB field at (a) $\mathcal{F}_{ISB} = 0$ eV, (b) $\mathcal{F}_{ISB} = 0.5[\varepsilon_{32} + \varepsilon_{12}]$, (c) $\mathcal{F}_{ISB} = \varepsilon_{32} + \varepsilon_{12}$, and (d) $\mathcal{F}_{ISB} = 2[\varepsilon_{32} + \varepsilon_{12}]$. The system is mostly gapped with the ISB field, in contrast to the in-plane magnetization field.

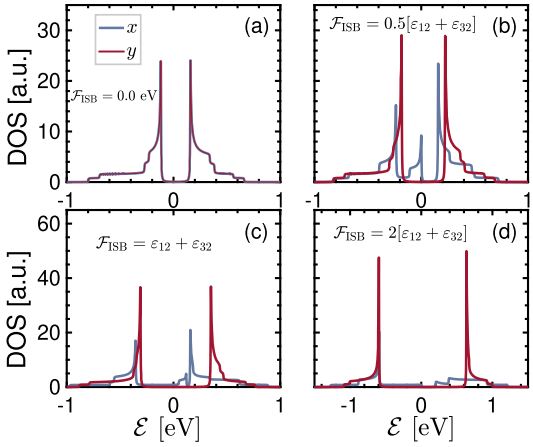

Fig. 5. Dressed electronic DOS of monolayer PbBiI by the ISB field at (a) $\mathcal{F}_{ISB} = 0$ eV, (b) $\mathcal{F}_{ISB} = 0.5[\varepsilon_{32} + \varepsilon_{12}]$, (c) $\mathcal{F}_{ISB} = \varepsilon_{32} + \varepsilon_{12}$, and (d) $\mathcal{F}_{ISB} = 2[\varepsilon_{32} + \varepsilon_{12}]$. In this mechanism, y-direction is the winner of flatter bands for weakest orbital hybridizations.

weakly overlap along the x-direction for $\mathcal{F}_M \leq \varepsilon_{32} + \varepsilon_{12}$, while this occurs along the y-direction for $\mathcal{F}_M > \varepsilon_{32} + \varepsilon_{12}$.

3.2. $\mathcal{F}_{ISB}$ effects

Given that the different types of vHs around the Fermi level originate from the CSB field, another field like $\mathcal{F}_{ISB}$ should show different novel features in monolayer PbBiI. We now investigate $\mathcal{F}_{ISB}$ effects on the vHs in Fig. 4(b)-(d) focusing on the same three regimes. While there are almost negligible effects in the conduction bands, valence bands, and the Fermi level contribute to novel insights for both bulk and RL gaps. We find that the majority of the effects come up with gap opening. It is necessary to point out that in the case of $\mathcal{F}_{ISB} = 0.5[\varepsilon_{32} + \varepsilon_{12}]$ in Fig. 4(b), the gapless phase in the valence band is not the bulk gap, but as a band-crossing effect between first and second bands, it occurs close to the Fermi level.

The most relevant number of vHs is then identical for all three regimes, except $\mathcal{F}_{ISB} = 0.5[\varepsilon_{32} + \varepsilon_{12}]$ due to the crossing of valence bands close to the Fermi level. The first regime, Fig. 5(b), exhibits three vHs along the x-direction, while one still finds two vHs along the y-direction such that y-direction vHs are flatter. In the second regime, Fig. 5(c), it is still safe to report two vHs along both directions. Similarly, y-directions provide the flatter vHs. In the x component of the third regime, Fig. 5(d), the vHs in the conduction band is weak and one would report one vHs along the x-direction, while two vHs along the y-direction still take place with the most flatness. In terms of bulk gap, increasing trend for $\mathcal{F}_{ISB} \geq \varepsilon_{32} + \varepsilon_{12}$ still holds true. Compared to the in-plane magnetization field $\mathcal{F}_M$, electrons dispersing along the y-direction provide flatter vHs in the presence of an ISB field. So, this shows that lattice sites overlap very weakly with the ISB field along the y-direction.

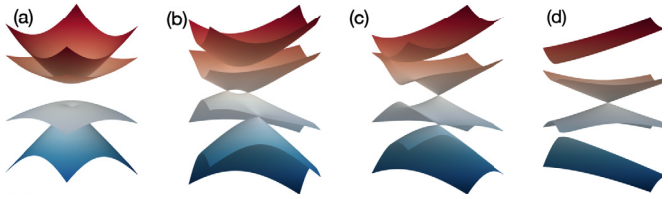

Fig. 6. Dressed band structure of monolayer PbBiI by the $\mathcal{F}$ field at (a) $\mathcal{F}=0$ eV, (b) $\mathcal{F}=0.5[\varepsilon_{32}+\varepsilon_{12}]$, (c) $\mathcal{F}=\varepsilon_{32}+\varepsilon_{12}$, and (d) $\mathcal{F}=2[\varepsilon_{32}+\varepsilon_{12}]$. Depending on the regime, more physical insights including the gapless phase and Weyl nodes can be extracted with a mixture of both previous mechanisms.

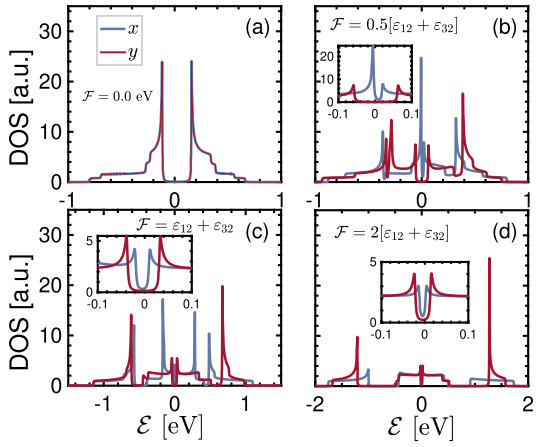

Fig. 7. Dressed electronic DOS of monolayer PbBiI by the $\mathcal{F}$ field at (a) $\mathcal{F}=0$ eV, (b) $\mathcal{F}=0.5[\varepsilon_{32}+\varepsilon_{12}]$, (c) $\mathcal{F}=\varepsilon_{32}+\varepsilon_{12}$, and (d) $\mathcal{F}=2[\varepsilon_{32}+\varepsilon_{12}]$. Upon applying a mixture of in-plane magnetization and ISB fields, orbitals start to overlap differently compared to the individual overlap structure of the two mechanisms.

3.3. $\mathcal{F}$ effects

We now study the effects of the applied $\mathcal{F}$ field, as a mixture of both in-plane magnetization and ISB fields. We have already verified the emergence of Weyl nodes in the band structure with $\mathcal{F}_{\mathrm{M}}$ (not with $\mathcal{F}_{\mathrm{ISB}}$) and we expect to have them with $\mathcal{F}$ as well. The $\mathcal{F}$ evolution of the band structure for monolayer PbBi is summarized in Fig. 6. In contrast to the Weyl nodes appeared with $\mathcal{F}_{\mathrm{M}}=\varepsilon_{32}+\varepsilon_{12}$, they appear with $\mathcal{F}<\varepsilon_{32}+\varepsilon_{12}$. Additionally, conduction bands never cross each other, while this was not the case with two fields separately. As the combined field becomes larger than the benchmark energy difference $\varepsilon_{32}+\varepsilon_{12}$, band crossing in the valence side disappears, while we observed it before with individual fields. A more interesting result is a nearly zero gap (we will show later in the electronic DOS that it is not completely zero) for $\mathcal{F}\geq\varepsilon_{32}+\varepsilon_{12}$, while zero single gapless phase was only possible before with $\mathcal{F}_{\mathrm{M}}<\varepsilon_{32}+\varepsilon_{12}$.

We focus next on tracking the change in energy (relative to the Fermi level) of the vHs in the electronic DOS. The alteration that these vHs experience under external $\mathcal{F}$ is shown in Fig. 7. In all three regimes, two vHs along the y-direction move close to the Fermi level (in a linear fashion) upon applied $\mathcal{F}$, and subsequently more vHs emerge at energies below and above the Fermi level such that we have five (four) vHs with $\mathcal{F}<\varepsilon_{32}+\varepsilon_{12}$ ($\mathcal{F}\geq\varepsilon_{32}+\varepsilon_{12}$). However, we find six (four) vHs with $\mathcal{F}=\varepsilon_{32}+\varepsilon_{12}$ (otherwise) along the x-direction. In terms of orbital overlap of lattice sites, flatter bands, i.e. weaker hybridizations, belong to the x- and y-direction, respectively, for $\mathcal{F}<\varepsilon_{32}+\varepsilon_{12}$ and $\mathcal{F}\geq\varepsilon_{32}+\varepsilon_{12}$. These results suggest that while the individual mechanisms (with their associated vHs) provide important electronic structure ingredients in monolayer PbBiI, the role of combined mechanisms cannot be disregarded, and even more physical insights than individual ones emerge.

4. Conclusions

We have used tight-binding and Green's function methods to investigate the electronic band structure and electronic DOS of monolayer PbBiI as a new family of QSHIs, and we tracked the evolution of the two vHs in the vicinity of the Fermi energy upon applying two fields, namely in-plane magnetization and ISB. When applying the in-plane magnetization field, a gapless phase and Weyl nodes appear and following this, the two vHs move away from the Fermi level. Upon applying an ISB field, we find mostly a gapped structure and the two vHs similarly move away from the Fermi level. However, a combination effect of both fields leads to an opposite trend as the two vHs move closer to the Fermi level. Overall, various flat bands emerge depending on the dispersion direction of electrons and the strength of fields, meaning that the mechanisms are highly orbitally selective. Our results are highly desirable for optoelectronic applications since the optical absorption spectrum of a system can be mainly determined by the band structure and the novel physical insights above-mentioned play important roles.

CRediT authorship contribution statement

Tran C. Phong: Writing – original draft, Visualization, Supervision, Software, Methodology, Investigation, Formal analysis, Data curation, Conceptualization. **Nguyen T. Nam:** Writing – original draft, Visualization, Software, Investigation, Formal analysis, Data curation. **Le T.T. Phuong:** Writing – review & editing, Writing – original draft, Visualization, Software, Methodology, Investigation, Formal analysis, Data curation.

Declaration of competing interest

The authors declare that they have no known competing financial interests or personal relationships that could have appeared to influence the work reported in this paper.

Data availability

Data will be made available on request.

References

[1] M.Z. Hasan, C.L. Kane, Rev. Mod. Phys. 82 (2010) 3045.
[2] X.-L. Qi, S.-C. Zhang, Rev. Mod. Phys. 83 (2011) 1057.
[3] B. Yan, S.-C. Zhang, Rep. Prog. Phys. 75 (2012) 096501.
[4] M. Yarmohammadi, M. Bukov, M.H. Kolodrubetz, Phys. Rev. B 107 (2023) 054439.
[5] C.L. Kane, E.J. Mele, Phys. Rev. Lett. 95 (2005) 226801.
[6] B.A. Bernevig, T.L. Hughes, S.-C. Zhang, Science 314 (2006) 1757.
[7] M. König, S. Wiedmann, C. Brüne, A. Roth, H. Buhmann, L.W. Molenkamp, X.-L. Qi, S.-C. Zhang, Science 318 (2007) 766.
[8] L. Kou, Y. Ma, Z. Sun, T. Heine, C. Chen, J. Phys. Chem. Lett. 8 (2017) 1905.
[9] S. Maekawa, S. Valenzuela, E. Saitoh, T. Kimura, Spin Current, Series on Semiconductor Science and Technology, OUP Oxford, 2012.
[10] A. Manchon, H.C. Koo, J. Nitta, S.M. Frolov, R.A. Duine, Nat. Mater. 14 (2015) 871.
[11] D. Bercioux, P. Lucignano, Rep. Prog. Phys. 78 (2015) 106001.
[12] J. Nitta, T. Akazaki, H. Takayanagi, T. Enoki, Phys. Rev. Lett. 78 (1997) 1335.
[13] T. Hirahara, T. Nagao, I. Matsuda, G. Bihlmayer, E.V. Chulkov, Y.M. Koroteev, P.M. Echenique, M. Saito, S. Hasegawa, Phys. Rev. Lett. 97 (2006) 146803.
[14] S. Mathias, A. Ruffing, F. Deicke, M. Wiesenmayer, I. Sakar, G. Bihlmayer, E.V. Chulkov, Y.M. Koroteev, P.M. Echenique, M. Bauer, M. Aeschlimann, Phys. Rev. Lett. 104 (2010) 066802.
[15] H. Yuan, M.S. Bahramy, K. Morimoto, S. Wu, K. Nomura, B.-J. Yang, H. Shimotani, R. Suzuki, M. Toh, C. Kloc, X. Xu, R. Arita, N. Nagaosa, Y. Iwasa, Nat. Phys. 9 (2013) 563.
[16] J.H. Dil, F. Meier, J. Lobo-Checa, L. Patthey, G. Bihlmayer, J. Osterwalder, Phys. Rev. Lett. 101 (2008) 266802.
[17] C. Mera Acosta, O. Babilonia, L. Abdalla, A. Fazzio, Phys. Rev. B 94 (2016) 041302.

[18] T. Phong, V.T. Lam, B.D. Hoi, J. Phys. Condens. Matter 33 (2021) 325502.
[19] B.D. Hoi, Phys. Rev. B 106 (2022) 165424.
[20] N.N. Hieu, C.V. Nguyen, H.V. Phuc, B.D. Hoi, T.C. Phong, Physica B, Condens. Matter 643 (2022) 414180.
[21] N.N. Hieu, B.D. Hoi, T.-N. Do, N.P. Anh, T.C. Phong, Phys. Lett. A 444 (2022) 128238.
[22] L.T.T. Phuong, T.C. Phong, B.D. Hoi, M. Yarmohammadi, J. Mater. Chem. A 10 (2022) 16620.
[23] A. Ström, H. Johannesson, G.I. Japaridze, Phys. Rev. Lett. 104 (2010) 256804.
[24] J.C. Budich, F. Dolcini, P. Recher, B. Trauzettel, Phys. Rev. Lett. 108 (2012) 086602.
[25] F.m.c. Crépin, J.C. Budich, F. Dolcini, P. Recher, B. Trauzettel, Phys. Rev. B 86 (2012) 121106.
[26] T.L. Schmidt, S. Rachel, F. von Oppen, L.I. Glazman, Phys. Rev. Lett. 108 (2012) 156402.
[27] J.I. Väyrynen, M. Goldstein, L.I. Glazman, Phys. Rev. Lett. 110 (2013) 216402.
[28] F. Geissler, F.m.c. Crépin, B. Trauzettel, Phys. Rev. B 89 (2014) 235136.
[29] K. Jiang, S. Zhou, X. Dai, Z. Wang, Phys. Rev. Lett. 120 (2018) 157205.
[30] B.A. Bernevig, T.L. Hughes, S.-C. Zhang, Science 314 (2006) 1757.
[31] M. König, S. Wiedmann, C. Brüne, A. Roth, H. Buhmann, L.W. Molenkamp, X.-L. Qi, S.-C. Zhang, Science 318 (2007) 766.
[32] M. König, H. Buhmann, L.W. Molenkamp, T. Hughes, C.-X. Liu, X.-L. Qi, S.-C. Zhang, J. Phys. Soc. Jpn. 77 (2008) 031007.
[33] B. Scharf, A. Matos-Abiague, J. Fabian, Phys. Rev. B 86 (2012) 075418.
[34] P. Debray, S.M.S. Rahman, J. Wan, R.S. Newrock, M. Cahay, A.T. Ngo, S.E. Ulloa, S.T. Herbert, M. Muhammad, M. Johnson, Nat. Nanotechnol. 4 (2009) 759.
[35] P. Chuang, S.-C. Ho, L.W. Smith, F. Sfigakis, M. Pepper, C.-H. Chen, J.-C. Fan, J.P. Griffiths, I. Farrer, H.E. Beere, G.A.C. Jones, D.A. Ritchie, T.-M. Chen, Nat. Nanotechnol. 10 (2015) 35.
[36] A.T. Ngo, P. Debray, S.E. Ulloa, Phys. Rev. B 81 (2010) 115328.
[37] N.A. Gokcen, J. Phase Equilib. 13 (1992) 21.
[38] H.W. Huang, C.M. Serrano, J. Vac. Sci. Technol. A 1 (1983) 1409.
[39] I.K. Drozdov, A. Alexandradinata, S. Jeon, S. Nadj-Perge, H. Ji, R.J. Cava, B. Andrei Bernevig, A. Yazdani, Nat. Phys. 10 (2014) 664.
[40] R. Yu, X.L. Qi, A. Bernevig, Z. Fang, X. Dai, Phys. Rev. B 84 (2011) 075119.
[41] A.A. Soluyanov, D. Vanderbilt, Phys. Rev. B 83 (2011) 035108.
[42] A.A. Soluyanov, D. Vanderbilt, Phys. Rev. B 83 (2011) 235401.
[43] M. Ezawa, Phys. Lett. A 379 (2015) 1183.
[44] A. Ullah, K. Sabeeh, J. Phys. Condens. Matter 26 (2014) 505303.
[45] M. Yarmohammadi, Phys. Lett. A 381 (2017) 1261.
[46] B.D. Hoi, M. Yarmohammadi, J. Magn. Magn. Mater. 451 (2018) 57.
[47] B.D. Hoi, M. Yarmohammadi, H.A. Kazzaz, J. Magn. Magn. Mater. 439 (2017) 203.
[48] M. Yarmohammadi, M.R. Ebrahimi, Phys. Rev. B 100 (2019) 165409.
[49] G. Mahan, Many-Particle Physics, Physics of Solids and Liquids, Springer, 2000.
[50] A. Chandrasekaran, A. Shtyk, J.J. Betouras, C. Chamon, Phys. Rev. Res. 2 (2020) 013355.
[51] N.F.Q. Yuan, L. Fu, Phys. Rev. B 101 (2020) 125120.
[52] D.V. Efremov, A. Shtyk, A.W. Rost, C. Chamon, A.P. Mackenzie, J.J. Betouras, Phys. Rev. Lett. 123 (2019) 207202.
[53] A. Chandrasekaran, J.J. Betouras, Phys. Rev. B 105 (2022) 075144.
[54] C. Herring, Phys. Rev. 52 (1937) 365.
[55] B.Q. Lv, H.M. Weng, B.B. Fu, X.P. Wang, H. Miao, J. Ma, P. Richard, X.C. Huang, L.X. Zhao, G.F. Chen, Z. Fang, X. Dai, T. Qian, H. Ding, Phys. Rev. X 5 (2015) 031013.
[56] L. Lu, Z. Wang, D. Ye, L. Ran, L. Fu, J.D. Joannopoulos, M. Soljačić, Science 349 (2015) 622.